Phytoplankton community structure in relation to iron and macronutrient fluxes from subsurface waters in the western North Pacific during summer

Huailin Deng[1,2], Koji Suzuki[2,3], Ichiro Yasuda[4], Hiroshi Ogawa[4], Jun Nishioka[1,2]

[1]Pan-Okhotsk Research Center, Institute of Low Temperature Science, Hokkaido University, Sapporo, 060-0819, Japan
[2]Graduate School of Environmental Science, Hokkaido University, Sapporo, 060-0810, Japan
[3]Faculty of Environmental Earth Science, Hokkaido University, Sapporo, 060-0810, Japan
[4]Atmosphere and Ocean Research Institute, The University of Tokyo, Chiba, 277-8564, Japan

Correspondence to: Huailin Deng (denghl@lowtem.hokudai.ac.jp), Jun Nishioka (nishioka@lowtem.hokudai.ac.jp)

Abstract. Iron (Fe) and macronutrient supplies and their ratios are major factors determining phytoplankton abundance and community composition in the North Pacific. Previous studies have indicated that Okhotsk Sea Intermediate Water and North Pacific Intermediate Water (NPIW) transport sedimentary Fe to the western subarctic Pacific. Although the supply of Fe and macronutrients from subsurface waters is critical for surface phytoplankton productivity, return paths from NPIW to the subsurface and their impact on the abundance and community composition of the organisms have not been fully understood. In this study, Fe and macronutrient turbulent fluxes, as well as the flux ratios from NPIW to surface waters, were calculated based on a chemical dataset, which included Fe and macronutrient concentrations, with turbulent mixing parameters obtained from the same cruise and same station along the 155° E transect in summer. Additionally, vertical flux divergence was calculated from the estimated vertical fluxes. Surface and subsurface phytoplankton community composition was evaluated in the CHEMTAX program based on algal pigment measurements. The results show that diatom abundance is significantly correlated with the vertical fluxes of Fe and macronutrients, especially with Fe and silicate (Si) fluxes, and with the Fe/N flux ratio along the section line. These results suggest that diatom abundance was controlled by Fe supply from subsurface waters in summer. The computed turbulent flux divergence in the subarctic and Kuroshio-Oyashio Transition Area suggests that enhanced concentrations of Fe and Si in the subsurface layer were supplied from NPIW.

1 Introduction

Iron (Fe) and nitrate supplies, as well as their ratios, are major factors for determining phytoplankton productivity in the North Pacific subarctic (Tsuda et al., 2003; Takeda, 2011) and subtropical (Rii et al., 2018) gyres, respectively. Diatoms and picocyanobacterium *Prochlorococcus* are dominant phytoplankton groups in the euphotic layer in the North Pacific subarctic (Suzuki et al., 2011; Endo et al., 2018) and subtropical gyres (Yun et al., 2020), respectively. To understand the factors controlling the supply of Fe and macronutrients, and how the supply would influence the phytoplankton communities, along with the abundance and composition of phytoplankton groups, need to be studied simultaneously.

The availability of Fe and macronutrients can influence the higher trophic organisms through primary producers (i.e., phytoplankton). According to FAO (2020), the western North Pacific accounts for 25% of the global fishery production. Therefore, it is essential to know the mechanisms of Fe and macronutrient supply and the associate response of phytoplankton communities. There are two primary Fe sources in surface waters of the oceanic western North Pacific: "aerosol Fe deposition" and "oceanic Fe supply". We need a coherent explanation for the biological response in the western North Pacific waters that incorporates knowledge of both. Mineral dust and anthropogenic aerosols from East Asia have been regarded as important Fe sources in the western North Pacific (Duce et al., 1991; Jickells et al., 2005; Ito et al., 2019; Kurisu et al., 2021). Although a few reports indicated that the dust supply stimulates phytoplankton growth in the subarctic Pacific (e.g., Bishop et al., 2002; Hamme et al., 2010), and the anthropogenic source of Fe has high bioavailability (Kurisu et al., 2024), dust-mediated biological production is still rare to be observed in the ocean because of sporadic aerosol Fe supply and scarce sampling opportunities

(Boyd et al., 2010). Therefore, oceanic Fe sources must be considered for the major biological production in the North Pacific (Nagashima et al., 2023).

45

For the oceanic Fe supply, previous studies indicated that Okhotsk Sea Intermediate Water and North Pacific Intermediate Water (NPIW) carry sedimentary Fe derived from the continental shelves to the western subarctic Pacific, which would further fuel oceanic phytoplankton productivity (Nishioka et al., 2007, 2013, 2020; Nishioka and Obata, 2017). The influence of NPIW can affect the intermediate water of the subtropical eastern North Pacific (Conway and John, 2015) and the subtropical western

50 North Pacific (Yamashita et al., 2020), which indicates that sedimentary Fe derived from the continental shelves could be distributed widely throughout the North Pacific. Nishioka et al. (2020, 2021) demonstrated that Fe and macronutrients were transported from NPIW to less dense water (< 26.6 σ_θ) by enhanced high vertical turbulent diapycnal mixing, which was generated by the interaction between tidal currents and rough topography around the marginal sea island chains. They also indicated that Fe might be transported upward from the shallower isopycnal surface of the upper NPIW (26.6 σ_θ) to the surface

55 layer by winter deep convective mixing.

Major macronutrients in subsurface waters can be transported to the surface layer by vertical turbulent diapycnal mixing in the western North Pacific (Rae et al., 2020; Holzer et al., 2021). Sarmiento et al. (2004) utilized a tracer named Si* ($Si(OH)_4 - NO_3^-$), which was prepared by combining silicate with nitrate, and concluded that the nutrient return path from the intermediate

60 layer to the surface layer is located in the northwest corner of the Pacific; moreover, NPIW might serve as an important nutrient source which retains the high Si* signature in the subsurface layer in both high- and low-latitude areas. Kaneko et al. (2021) asserted that vertical nitrate transportation occurs from NPIW to the surface layer in the Emperor Seamount with prominent divergence/convergence features, and the nitrate return path might be located in the subtropical Pacific, as internal tides would elevate vertical flux locally. Elevated vertical turbulent nitrate flux was observed in the Kuroshio area, which might imply

65 nitrate transportation from NPIW (Nagai et al., 2019; Tanaka et al., 2019).

To date a few studies have confirmed the relationships between Fe or macronutrient supply fluxes and biological responses. It is noteworthy that the phytoplankton abundance in the western North Pacific varies seasonally (Shimada et al., 2006; Hashioka and Yamanaka, 2007; Nishioka et al., 2011; Takahashi et al., 2013; Nishioka et al., 2021), therefore, we need to understand

70 which Fe supply processes are controlling the seasonal variation of phytoplankton abundance and taxonomy. In this study, we mainly focused on the oceanic Fe supply process and quantitatively examined the Fe supply by estimating Fe and macronutrient fluxes from subsurface waters toward the surface and then investigated their relationships with phytoplankton community composition as estimated from the pigment data during summer. In addition, the mechanisms and location of the Fe and macronutrient return path from NPIW to the subsurface layer were evaluated.

2 Data and methods
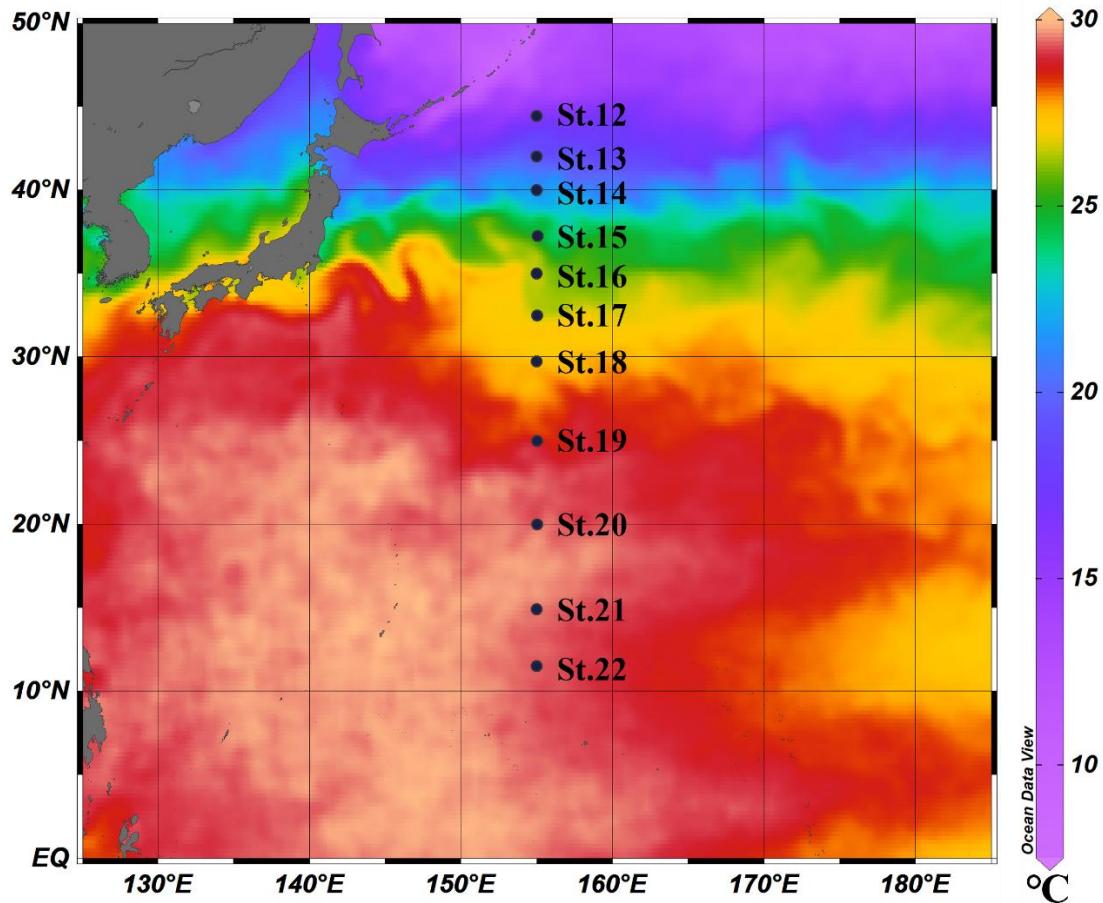
Figure 1: Location of observed stations from St. 12 to St. 22 in the cruise of KH-08-2. The sea surface temperature (SST) data was cited from NOAA Daily Optimum Interpolation Sea Surface Temperature (OISST) V2.1 High Resolution Dataset (https://www.ncei.noaa.gov/products/optimum-interpolation-sst) (Huang et al., 2021). This figure used the average SST data calculated from August 1st to September 9th, 2008, and was drawn using the software Ocean Data View (ODV; Schlitzer, R., Ocean Data View, http://odv.awi.de, 2016).

Observation and sample collection were conducted in the western North Pacific during the KH-08-2 expedition of the R/V *Hakuho-maru* (JAMSTEC/ U. Tokyo) from August 1st to September 9th, 2008. All the stations were arranged on a 155° E transect from 40° N to 11.5° N (Fig. 1). For the data used in this study, a chemical dataset was obtained from Nishioka et al. (2013, 2020), and a physical dataset was obtained from Kaneko et al. (2021).

Hydrography data, including salinity and *in situ* temperature, were measured using a conductivity–temperature–depth (CTD; SBE911plus; SeaBird Electronics Inc.) sensor. Station (hereafter, St.) 12 was located in the subarctic gyre (SAG) between the

subarctic front and subarctic boundary. The subarctic front is defined as where the *in situ* temperature is approximately 4 °C at 100 m depth, and salinity decreases upward (Favorite, 1976). In the subarctic boundary, surface salinity approaches 34.0 (Favorite, 1976). The Kuroshio-Oyashio Transition Area (KOTA) is between the subarctic boundary and the Kuroshio Extension (KE), and the KE is marked as the location at which the temperature is approximately 14 °C at 200 m depth (Kawai, 1969). St.13-15 and St. 16-17 were located in the KOTA and KE, respectively. The subtropical gyre (STG) is south of the KE, where St.18-22 were located.

The chemical dataset used in this study, including dissolved Fe (dFe) and macronutrient (nitrate, phosphate, and silicate) concentrations during the R/V *Hakuho-Maru* KH-08-2 cruise, has already been published (Nishioka et al., 2013, 2020). The chemical dataset includes data on discrete water samples collected from the surface to the bottom (bottom depth 4400−5600 m). The dFe concentrations were determined with a flow-injection analysis (FIA) system (Obata et al., 1993), which was quality-controlled by the SAFe reference sample (Johnson et al., 2007). Macronutrient concentrations were measured by a BRAN-LUEBBE autoanalyzer (TRACCS 800).

The physical dataset used in this study, including vertical turbulent mixing parameters obtained from the same cruise and same stations as chemical parameter measurements, ranging from the surface to approximately 2000 m depth, has been reported in Kaneko et al. (2021). The turbulent energy dissipation rate (ε) was measured based on microscale velocity fluctuations derived from a vertical microstructure profiler (VMP2000; Rockland Scientific International Inc.). This method followed the procedure outlined by Itoh et al. (2010), who calculated shear spectra for segments lasting 16 seconds. The integration of these spectra across different wavenumbers yielded the value of ε. The vertical diffusivity ($K\rho$) used in this study was obtained from Kaneko et al. (2021), which was evaluated from the following formula:

$$K\rho = \varepsilon \, \Gamma / N^2, \tag{1}$$

where the turbulent kinetic energy dissipation rate (ε) was measured by a VMP2000, the mixing efficiency (Γ) was assumed to be a constant 0.2 (Osborn, 1980), and the square of buoyancy frequency (N^2) was calculated as $N^2 = -g/\rho_0 \, \partial\sigma_\theta/\partial Z$, where g and ρ_0 are the gravitational acceleration and reference potential density, based on Kaneko et al. (2013). As there was large variation in the turbulence, $K\rho$ value was calculated at every 50 m depth to increase the estimation accuracy (Kaneko et al., 2013).

The dFe and macronutrient vertical turbulent flux (F) were quantified by the following formula (Kaneko et al., 2021):

$$F = -K_\rho \frac{\partial C}{\partial Z} \text{ (Lewis et al., 1986) (minus indicated upward flux)}, \tag{2}$$

where K_ρ and $\frac{\partial C}{\partial Z}$ indicate vertical diffusivity and dFe or macronutrient vertical gradient, respectively.

The dFe and macronutrient fluxes are displayed in two ways: 1) flux for the section profile and 2) individual flux (henceforth 'indiv-flux') for the vertical profile at each station. 1) Flux for the section profile represents the vertical flux within the entire section, where this flux was calculated with the vertical gradients of dFe and macronutrient concentrations ($\frac{\partial C}{\partial Z}$) between every adjacent two discrete water samples depths of the water column, and the vertical diffusivity in the corresponding shallower layer. 2) For the calculation of the indiv-flux, vertical gradients of dFe and macronutrient concentrations ($\frac{\partial C}{\partial Z}$) were calculated from the layer where the concentration changed sharply with depth below the surface (calculation details and selected depth range are shown in Supplement Fig. S1, S2, respectively). The average K_ρ value was used in the same depth range. Also, the flux ratios (such as the dFe/N flux ratio) were calculated as the ratio of two indiv-fluxes within the same depth range at each station. Flux for the 1) section profile is used to display the distributions of the fluxes and to calculate the flux divergences; 2) indiv-flux is used to compare it with biological parameters in each station.

Additionally, vertical flux divergence was calculated from the equation below based on Kaneko et al. (2021):

$$Flux\ divergence = \frac{F_{Z1} - F_{Z2}}{Z_1 - Z_2}, \tag{3}$$

where Z_1 and Z_2 represent the upper and lower depths of every two fluxes for the section profile (0 m < Z_1 < Z_2). F_{Z1} and F_{Z2} were the fluxes for the section profile at the depths of Z_1 and Z_2.

Divergence occurs when the value of flux divergence is positive, indicating that upward nutrient flux in the upper layer is larger than in the lower layer. The total nutrient concentration in the corresponding layer decreases where positive divergence is indicated. On the other hand, convergence occurs when the value of the flux divergence is negative and the total nutrient concentration in the corresponding layer increases (details are shown in Supplement Fig. S3).

Biological parameters, including chlorophyll a (Chl a) and other pigment concentrations, were also measured at the same stations during the cruise, and the depth range was from the surface to 150 m depth. Chl a concentration was measured onboard with a Turner Designs fluorometer AU-10 using the non-acidification method of Welschmeyer (1994). The subsurface Chl a maximum (SCM) was evaluated from Chl a data in vertical profiles. The vertically integrated Chl a concentration (VIC: unit is mg/m^2) was calculated based on a trapezoidal rule of the data from the surface to 150 m. Chlorophylls and carotenoids were also analyzed by high-performance liquid chromatography (HPLC) according to Suzuki et al. (2014, 2021). In brief, duplicate 2.0-2.4 L seawater samples collected with acid-cleaned 12-L Niskin-X bottles were filtered onto Whatman GF/F filters (nominal pore size 0.7 μm, 25 mm in diameter) under a low-vacuum (<0.013 MPa) pressure. The filtered samples were then stored in a deep freezer (–80 °C) prior to onshore analysis. The frozen filter was minced and soaked in 3 mL DMF (N, N-dimethyl formamide), and canthaxanthin was added as an internal standard. The pigment extracted by DMF was filtered using 0.45-μm PTFE filters to remove fine particles. A 250 μL mixture of pigment extracts and 1 M ammonium acetate solution were introduced into an HPLC system (CLASS-VP System, Shimadzu) along with an Agilent ZORBAX Eclipse XDB-C8

Rapid Resolution column (3.5 μm particle size, 4.6 × 150 mm) connected to an Agilent Eclipse XDB-C8 cartridge (3.5 μm particle size, 4.6 × 30 mm) as the guard column. Based on pigment concentration and composition, phytoplankton community composition was estimated with the CHEMTAX (version 1.95) program (Mackey et al., 1996). Total Chl *a* biomass was set by the sum of HPLC-determined Chl *a* and divinyl Chl *a* (DV Chl *a*) derived from *Prochlorococcus* (Suzuki et al., 1995). For the CHEMTAX analysis, precise estimation requires that the initial ratios are close to those of the assessed phytoplankton assemblage (Latasa, 2007). The initial pigment ratio matrix of Chl *a* for eight taxonomic groups, including diatoms, dinoflagellates, chlorophytes, prasinophytes, chrysophytes, haptophytes, and cyanobacteria (excluding *Prochlorococcus*), and that of DV Chl *a* for *Prochlorococcus* were selected and modified from Kanayama et al. (2020) during CHEMTAX analysis. The ratio limit was set to 500% to constrain all the pigment calculations (Mackey et al., 1996). To derive the most suitable matrix of phytoplankton community composition, 60 further pigment ratio matrices were introduced (scaling factor = 0.7) based on the initial matrix, and the 6 matrices with the smallest root-mean-square error (RMSE) were selected. The average matrix of these 6 matrices was regarded as the final matrix (scaling factor = 0.7) and initial matrix for the next run (scaling factor = 0.4). The same procedure was performed, and the second average matrix was chosen for the phytoplankton community composition calculation after comparison (details are shown in Supplement Tables S1-S3).

3 Results and discussion

3.1 Hydrographic conditions

High concentrations of dFe and macronutrients in NPIW have previously been reported by Nishioka et al. (2013, 2020). Yasuda et al. (2001) proposed that NPIW, with a core density of 26.8 σ_θ, can be divided into the upper NPIW (U-NPIW) and the lower NPIW (L-NPIW), whose main components are derived from Okhotsk Sea water (OSW) and the Western Subarctic Gyre (WSAG) water, respectively. According to Yasuda et al. (2001), the U-NPIW (density range is from 26.6 to 27.0 σ_θ) consisted of 71% OSW and 29% WSAG water, whereas the L-NPIW (density range is from 27.0 to 27.5 σ_θ) accounted for 75% WSAG and 25% OSW in the vicinity of the south coast of Hokkaido. Figures 2a and 2b show observed *in situ* temperature and salinity, respectively. The hydrographic data of this study clearly shows the stratification of water masses, indicating the U-NPIW. Particularly in Fig. 2b, the U-NPIW was identified by the vertical salinity minimum (Reid, 1965). In the SAG and KOTA, the 26.5 σ_θ isopycnal surface reaches ~100 m depth and extends to ~600 m in the STG. The low salinity intrusion from the subarctic to the subtropical region is observed in the U-NPIW isopycnal surfaces.
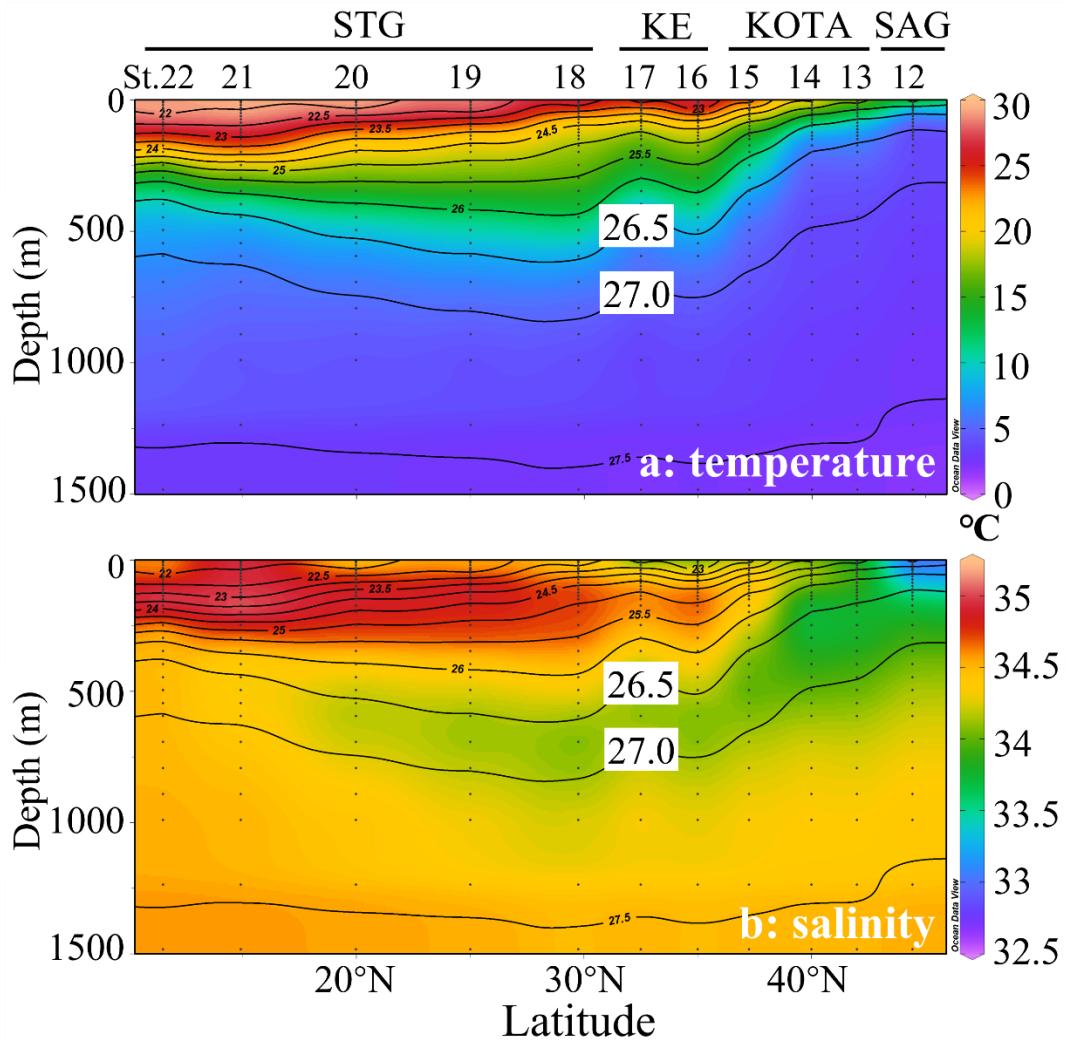
Figure 2: Section profiles of (a) in situ temperature (°C) and (b) salinity along the observational transect at 155° E from the subarctic gyre to the subtropical gyre. *SAG*: subarctic gyre, *KOTA*: Kuroshio-Oyashio Transition Area, *KE*: Kuroshio extension, *STG*: subtropical area. Black contour lines in the figures denote each potential density (σ_θ) with special reference to the 26.5 and 27.0 σ_θ isopycnal surfaces. In Figure 2b, the salinity minimum between the 26.5 - 27.0 σ_θ indicates the presence of U-NPIW. These figures were drawn using the ODV.

3.2 Turbulent mixing

As shown in Fig. 3, K_ρ varied from $O(10^{-4})$ m^2 s^{-1} to $O(10^{-7})$ m^2 s^{-1} (O stands for the order of magnitude). K_ρ was high, $O(10^{-5})$ m^2 s^{-1} below 26.5 σ_θ in the SAG, KOTA, and KE. In the SAG and KOTA, relatively high K_ρ of $O(10^{-5})$ m^2 s^{-1}, was observed in the water with a density greater than 26.5 σ_θ, which was ~ 200 m at St. 12, 13,14 and was ~ 400 m at St. 15. Whereas, in the STG, K_ρ was not as high and $O(10^{-6})$ m^2 s^{-1} between 26.5 σ_θ and 27.0 σ_θ, while K_ρ was $O(10^{-5})$ m^2 s^{-1} in the density >27.0 σ_θ,

195 which was at ~ 600 m depth. In the surface layer, K_ρ was low, $O(10^{-7})$ m^2 s^{-1} in the northern part, while high K_ρ, $O(10^{-5}$ to$10^{-4})$ m^2 s^{-1}, was observed at St. 20, 21, and 22 in the STG.
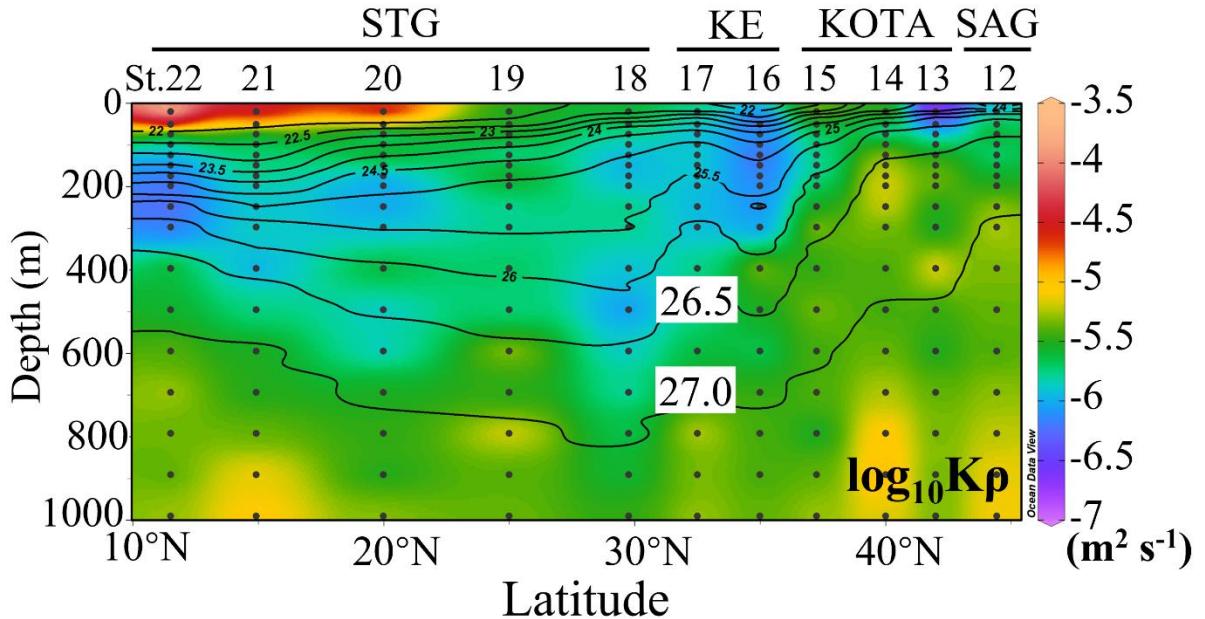
Figure 3: Vertical section profile of vertical diffusivity ($K\rho$) along the 155° E transect from the subarctic to the subtropical Pacific.
200 **Black contour lines in the figure denote each potential density (σ_θ) with special attention to the 26.5 and 27.0 σ_θ isopycnal surfaces. This figure was drawn using the ODV.**

3.3 Dissolved iron and macronutrient distribution

The vertical section profiles of dFe and macronutrient concentrations along the 155° E transect are shown in Fig. 4. In the
205 SAG, KOTA, and KE, high-dFe water (> 0.6 nM) was observed below the 26.5 σ_θ isopycnal surface and reached ~1 nM below the 27.0 σ_θ isopycnal surface. Particularly in the SAG and the KOTA, high dFe concentrations and steep gradient characteristics were found just below the surface layer (~ 100 m at the SAG station, ~ 200 m in the KOTA). In the STG, high-dFe water and a steep gradient are not observed just below the surface, but a high concentration (> 0.5 nM) is found in the deep layer with a density > 27.0 σ_θ.
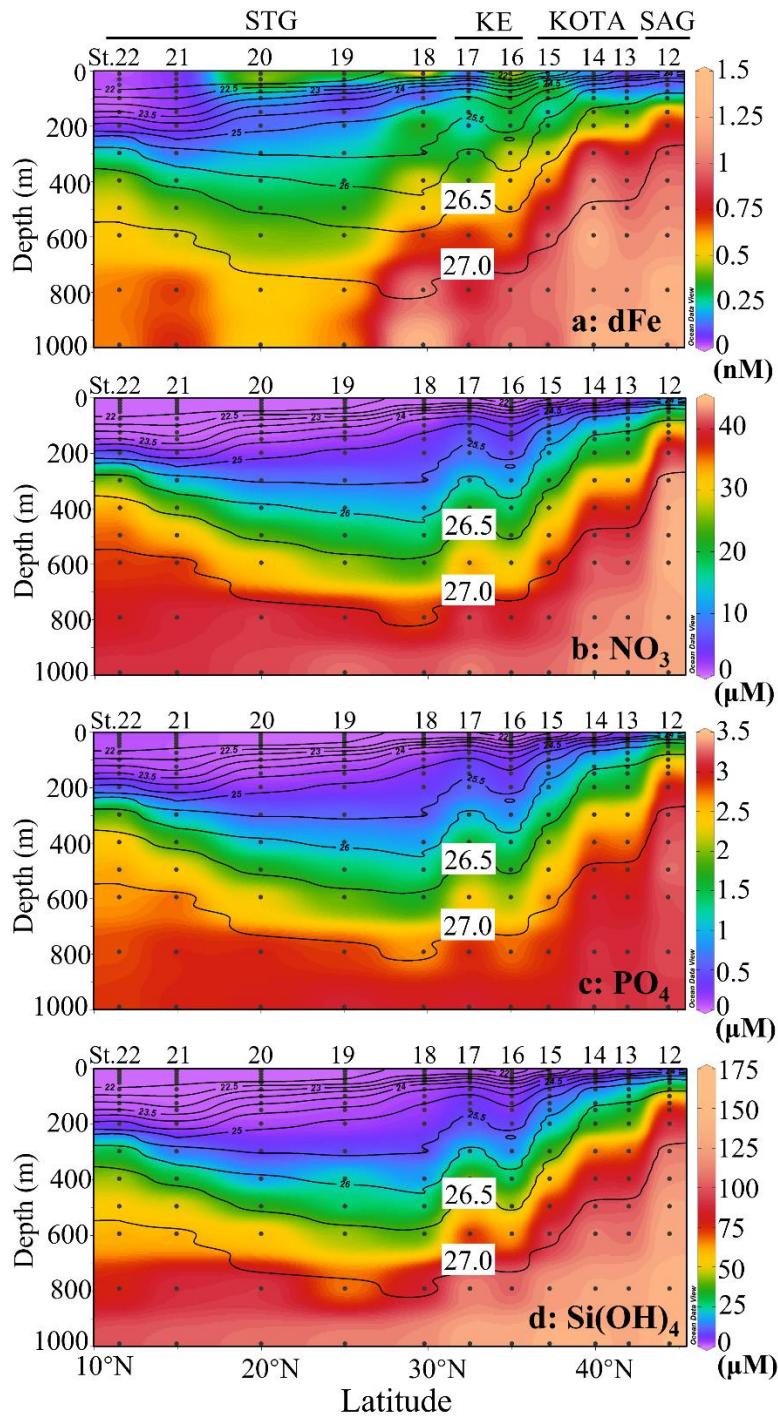
Figure 4: Vertical section profiles of (a) dissolved Fe, (b) nitrate, (c) phosphate, and (d) silicate concentration along 155° E transect from the subarctic to subtropical Pacific. Black contour lines in the figure denote each potential density (σ$_θ$) with special attention to the 26.5 and 27.0 σ$_θ$ isopycnal surfaces. This figure was drawn using the ODV.

210

Note that the macronutrient concentrations follow the isopycnal surface distribution strictly (macronutrient concentrations tend to be uniform along isopycnal surfaces) and increase with density, indicating that the dynamics of macronutrients are controlled by the water mass distribution and circulation. If NPIW reaches low-latitude areas, the macronutrients would also be transported that far. A high macronutrient concentration core (i.e., nitrate concentration with > 20 μM) deeper than 26.5 σ_θ, extends to the STG. On the other hand, the high-dFe concentration core in the density > 27.0 extends from the SAG to 30° N (St. 18). In contrast to the macronutrient, the high-dFe concentration core does not strictly follow the isopycnal surface distribution. This may be because part of the dFe fraction can be removed by sinking, scavenging, and aggregation during the lateral transport of NPIW (Yamashita et al., 2020; Misumi et al., 2021). Increased dFe is observed near the surface at St. 16, 18, and 20, but macronutrients are deficient. The result indicates that the surface layer of the KE and STG have a relatively high dFe concentration of ~0.5 nM, which could be caused by the supply from the upstream Kuroshio and/or aerosol Fe input (Kurisu et al., 2021).

3.4 Dissolved iron and macronutrient flux

The flux for the section profile was calculated from the adjacent two depths (Fig. 5). In the layer between the 26.0 and 27.0 σ_θ pycnocline, the upward dFe flux remains high, $O(-10^{-8})$ μmol m^{-2} s^{-1}, in the SAG and KOTA because both the vertical gradient of dFe concentration and vertical diffusivity are large. In the same density range (26.0−27.0 σ_θ) of the KE and STG, a lower upward dFe flux of $O(-10^{-10})$ μmol m^{-2} s^{-1} is observed because of a smaller dFe concentration gradient and a smaller vertical diffusivity in these regions. Near the surface at St. 20, 21, and 22 in the STG, an elevated upward dFe flux of $O(-10^{-7})$ μmol m^{-2} s^{-1} is observed mainly because of the high vertical diffusivity. Additionally, in the surface or subsurface layers at St. 15, 18, 19, and 20, the downward dFe flux of $O(10^{-9}-10^{-7})$ μmol m^{-2} s^{-1} is seen because of the higher dFe concentration at shallower depths (Fig. 4a).

In the water with a density lower than 27.0 σ_θ in the SAG and KOTA, a high upward nitrate flux of $O(-10^{-7})$ mmol m^{-2} s^{-1} is observed. Between the 25.5 and 27.0 σ_θ isopycnal surface in the KE and STG, a relatively high nitrate flux of $O(-10^{-8}--10^{-7})$ mmol m^{-2} s^{-1} is observed. In the surface layer of the STG, nitrate flux is seldom detected because the nitrate concentration is under the detection limit. The phosphate flux displays a similar pattern as the nitrate flux. However, there are distinct patterns between the nitrate and silicate flux in the water with a density greater than 27.0 σ_θ; higher upward silicate flux is observed, while nitrate flux is downward.
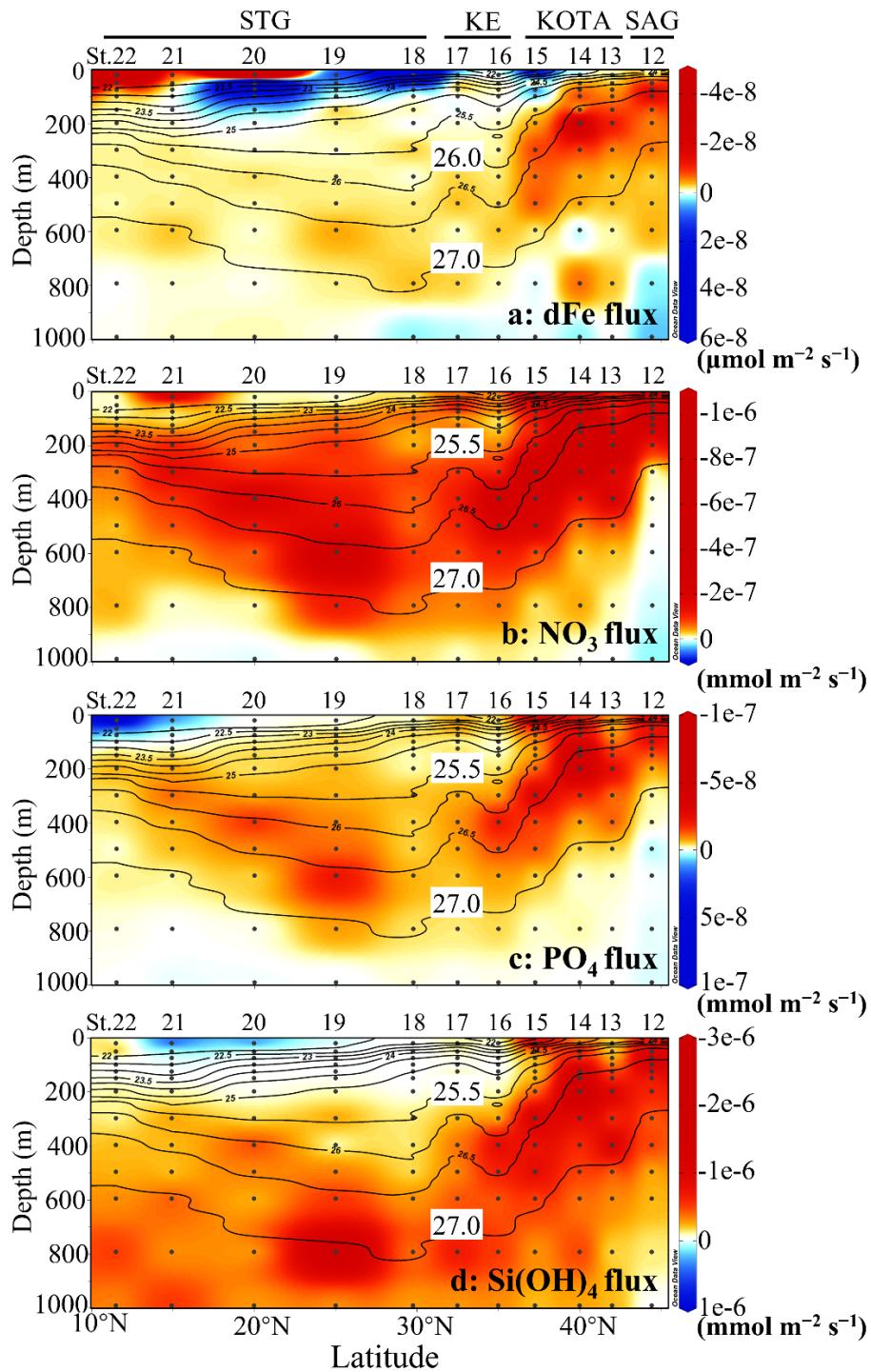
Figure 5: Vertical section profile of (a) dissolved Fe flux, (b) nitrate flux, (c) phosphate flux, and (d) silicate flux along 155° E transect from the subarctic to subtropical Pacific. Black contour lines in the figure denote each potential density (σθ) with special attention to the 25.5 or 26.0 and 27.0 σθ isopycnal surfaces. Upward-directed flux values are negative. This figure was drawn using the ODV.

245

3.5 Relationship between Chl *a* concentration and individual flux or flux ratio

Kaneko et al. (2021) compared sensor-based Chl *a* concentration (SCM and VIC) with nitrate flux calculated at the bottom of the euphotic zone at the same stations during the same cruise as in the present study. Consequently, they concluded that there was no clear relationship between the nitrate flux and Chl *a* concentration. In this study, the Chl *a* concentration (SCM and VIC) determined by HPLC were compared with dFe, nitrate, phosphate, silicate indiv-fluxes, and flux ratios. As a result, there is nearly no correlation between total Chl *a* concentration and individual fluxes or flux ratios (Supplement Fig. S4-S6). However, as the dominant phytoplankton communities would vary between the subarctic and subtropical Pacific, relationships between the phytoplankton community composition and dFe or macronutrient fluxes would attract more attention.

3.6 Relationship between Chl *a* concentration from each phytoplankton group and individual flux or flux ratio

The subsurface Chl *a* biomass maximum of each phytoplankton group along the 155° E was estimated with the CHEMTAX program using algal pigment data, as shown in Fig. 6a. Fig. 6b illustrates dFe and macronutrient indiv-fluxes. In the SAG and KOTA, the dFe and macronutrient indiv-fluxes are higher than those in the KE and STG. However, as shown in Fig. 6c, the dFe/N flux ratio is higher in the SAG and KOTA than in the KE and STG. Little difference is found in the other flux ratios among regions.

The distribution patterns of diatom-derived Chl *a* concentration and the subsurface diatom-derived Chl *a* maximum (SDM) are shown in Fig. 7a and 7b, respectively. Higher diatom-derived Chl *a* concentrations (~ 0.1 mg m^{-3}) are observed in the SAG above 100 m depth. In general, the SDM increases with latitude. The results of diatom distribution along 155° E in this study are similar to those of previous studies (Hirata et al., 2011; Endo et al., 2018; Li et al., 2023), which can provide more insights on the ecology of the organisms. Diatom abundance, as estimated from the 18S rRNA gene copy numbers, reached the maximum in the SAG and showed similar distribution patterns along 160° E in summer (Endo et al., 2018). Additionally, satellite-based diatom-derived Chl *a* concentration reported by Hirata et al. (2011) and Li et al. (2023) also increased with latitude in the western North Pacific. These studies would help contextualize our findings within the regional diatom dynamics.

Figure 6: Latitudinal distribution patterns of (a) subsurface chlorophyll *a* biomass maximum (mg/m³) of phytoplankton groups, including diatoms, prasinophytes, haptophytes, cyanobacteria (except *Prochlorococcus*), chrysophytes, dinoflagellates, *Prochlorococcus*, and chlorophytes in terms of chlorophyll *a* (Chl *a*) biomass (b) dissolved Fe and macronutrient indivi-fluxes and (c) dissolved Fe and macronutrient flux ratio.

270
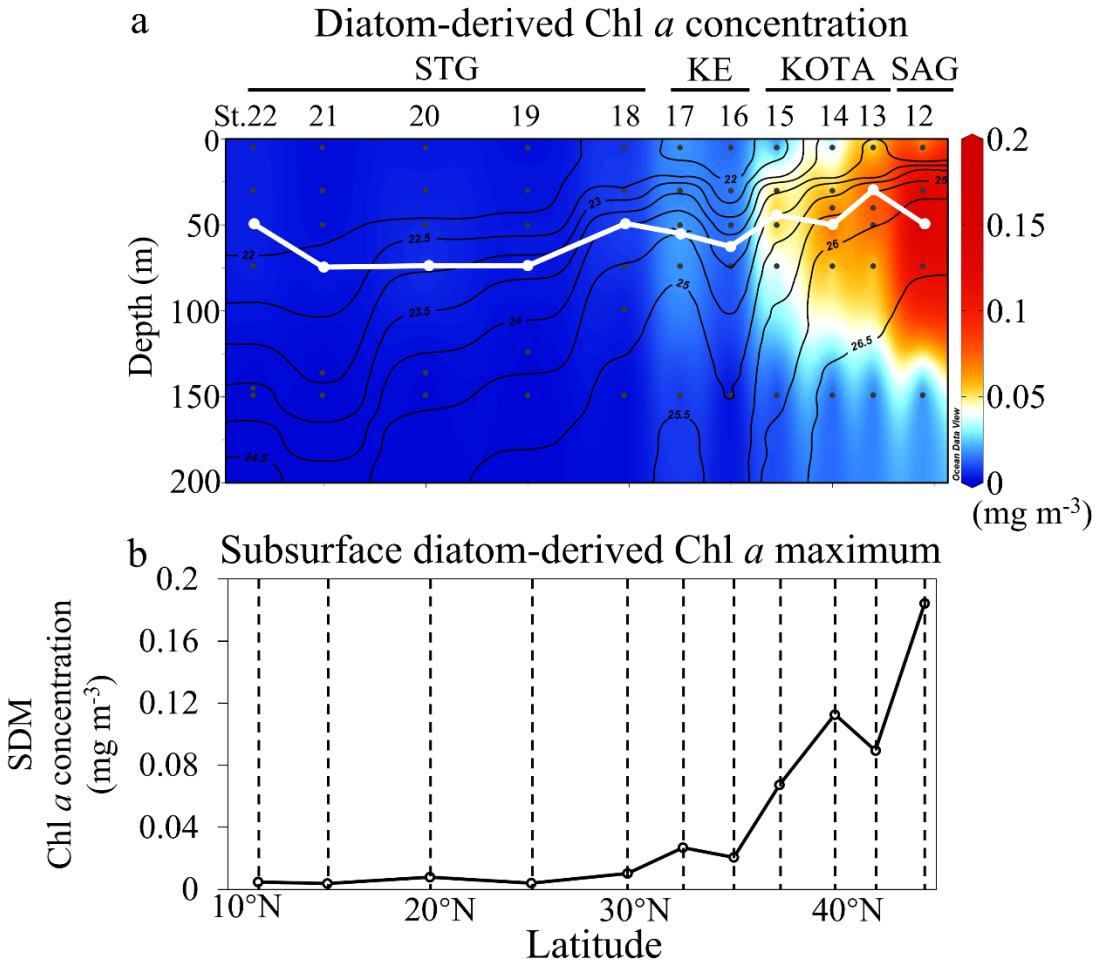
Figure 7: Section profiles of (a) diatom-derived Chl *a* concentration (mg m⁻³), (b) the subsurface diatom-derived Chl *a* maximum (SDM) concentration (mg m⁻³) at each station. In Figure 7a, the white line indicates the depth of SDM. Figure 7a was drawn using the ODV.

The SDM can be observed at the depth range of 30–75 m at all stations in this study. The depth range of indiv-fluxes, which indicated the nutrient supply from the subsurface, included the depth of SDM in the SAG, KOTA, KE, and some stations in the STG (St. 12–19). In the rest stations in the STG, indiv-fluxes were calculated just below the depth of SDM, from ~200 m depth at St. 20–21 and from ~150 m depth at St. 22. Pearson correlation analysis was employed to explore the relationships between dFe flux, macronutrient fluxes, and phytoplankton abundance, with the coefficient of determination (r^2) and p-value. As a result, linear correlations were found between the SDM and dFe or macronutrient indiv-fluxes (Fig. 8a–8d). These results indicate that the diatom abundance is highly controlled by dFe and macronutrient supply from the subsurface below. Based on the values of r^2 and p-values, dFe and Si fluxes are more highly correlated with diatom-derived Chl *a* concentration than nitrate

and phosphate, indicating that dFe and Si fluxes had higher impacts on the diatom abundance. For the flux ratios, the dFe/N flux ratio is correlated with the diatom-derived Chl *a* concentration (Fig. 8e–8h). Previous studies have proven that diatom growth was often limited by nutrient supply (Allen et al., 2005), including dFe (Hogle et al., 2018; Nishioka et al., 2021). Martin and Fitzwater (1988) demonstrated that Fe addition would stimulate the phytoplankton growth in the high nutrient-low chlorophyll (HNLC) area through an on-deck incubation experiment. Since then, a number of ocean in situ Fe fertilization experiments (Coale et al., 1996; Boyd et al., 2000; Tsuda et al., 2003; Boyd et al., 2004; Coale et al., 2004) and Fe-addition bottle incubation experiments (Martin et al., 1990; Hutchins and Bruland, 1998; Nodwell and Price, 2001; Hassler and Schoemann, 2009; Nishioka et al., 2009) were performed. These bioavailable Fe assays proved the role of Fe for diatom growth. Compared to other phytoplankton groups, the requirement of Fe and macronutrients in diatom is higher due to their larger cell size (Sunda and Huntsman, 1995). Also, the Fe starvation–induced protein 1 (ISIP1), which evolves in the Fe uptake process, is primarily a specific protein for diatoms (Kazamia et al., 2018). Different from other phytoplankton communities, diatoms form the silicified frustules that protect them against predators (Hamm et al., 2003), and diatoms with high nutrient uptake and high growth rate characteristics would utilize nutrients quickly for enhanced growth (Sommer, 1984; Litchman et al., 2007). As a result, dFe and macronutrient fluxes from subsurface waters control diatom abundance, especially dFe flux in summer. Contrasted to the winter season when winter deep mixing brings nutrients from the subsurface to the surface layer, eddy diffusion is one of the important physical processes that supply the nutrients from the subsurface to the surface in summer (Itoh et al., 2021).
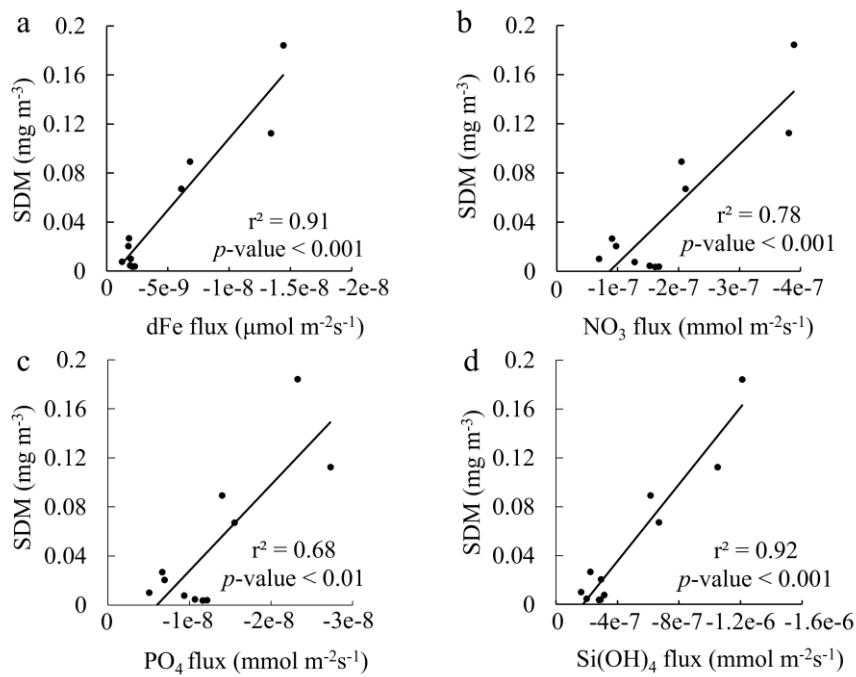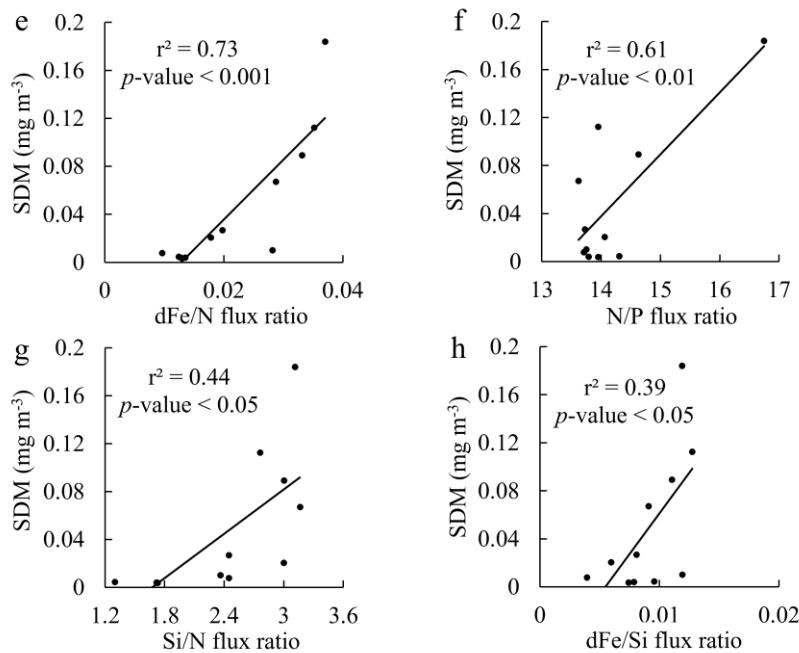
The Pearson correlation coefficient (r) between the subsurface Chl *a* maximum derived from each phytoplankton species and

315 dFe or macronutrient indiv-fluxes (shown in Fig. 9) indicates that diatoms, followed by haptophytes, prasinophytes are highly

positively correlated, and *Prochlorococcus* is negatively correlated, with dFe and macronutrient indiv-fluxes from subsurface

waters (r > 0.4).
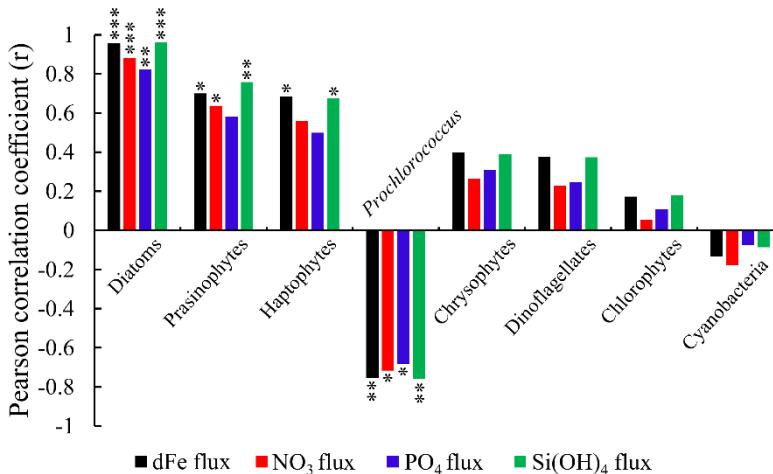
Figure 9: The Pearson correlation coefficient (r) between the subsurface Chl *a* maximum concentration of each phytoplankton group, dissolved Fe, and macronutrient indiv-fluxes (***p-value <0.001, **p-value <0.01, *p-value <0.05). Note that *Prochlorococcus* and other cyanobacteria are negatively correlated to indiv-fluxes, whereas other phytoplankton groups are positively correlated with indiv-fluxes.

Previous studies indicated that haptophytes dominated phytoplankton communities in the subtropical and subarctic North Pacific (Hirata et al., 2011), especially in the Kuroshio ecosystems (Endo and Suzuki, 2019). According to Wang et al. (2022), haptophyte abundance in the KOTA increased in proportion to nutrient supply and was markedly high in the KE in the depth of subsurface chlorophyll maximum, which is similar to the haptophyte distribution in this study, as shown in Fig. 6a. The haptophyte cell abundances were higher in the Fe addition treatments than those in the control treatments through the incubation studies (Endo et al., 2017). Nitrate addition stimulated the carbon fixation rates of haptophytes in nitrate-depleted waters (Mills et al., 2020). The haptophyte community composition was positively correlated with nitrate plus nitrite and phosphate concentrations by redundancy analysis with seawater samples collected across the Tokara Strait (Endo and Suzuki, 2019). In the haptophyte *Hyalolithus neolepis* occurring in the subarctic western Pacific, one scale type of the non-motile form undergoes intracellular silicification (Yoshida et al., 2006), suggesting a silica requirement. These studies coincide with the result of this study, which is that haptophyte abundance is controlled by the dFe and macronutrient fluxes from the subsurface.

Prasinophytes were predominant in the phytoplankton assemblage in the western SAG during summer (Suzuki et al., 2002). During the Subarctic Pacific Fe Experiment for Ecosystem Dynamics Study (SEEDS II), prasinophytes were predominant in the phytoplankton communities in the Fe-fertilized patch in the western North subarctic Pacific (Suzuki et al., 2009). A numerical modelling study indicated that prasinophytes were limited by Fe supply in the HNLC region of the subarctic Pacific (Litchman et al., 2006). Nitrate and phosphate supply stimulated the growth of prasinophyte *Micromonas* sp. and *Tetraselmis suecica* (a genus of prasinophytes), respectively, through the incubation experiment (Laws et al., 2011; Liefer et al., 2018). These studies indicate that prasinophyte abundance is limited by Fe and macronutrient availability, which agrees with this study that prasinophyte abundance is impacted by the dFe and macronutrient fluxes from the subsurface.

Fig. 9 indicates the negative correlations between *Prochlorococcus* abundance and nutrient fluxes. The negatively correlated results indicated that the *Prochlorococcus* abundance may be controlled by other factors. In Fig. 6a, *Prochlorococcus* is predominant in the STG and rare in the SAG. Previous studies indicated that *Prochlorococcus* abundance increases with temperature because of their higher metabolic rates (Sarmiento and Gruber, 2006). *Prochlorococcus* cells are seldom observed where the temperature is below 15 °C (Johnson et al., 2006). Also, high *Prochlorococcus* abundance was accompanied by low nutrient supply in subtropical regions (Zubkov et al., 2000). Yun et al. (2020) also reported that *Prochlorococcus* dominated the phytoplankton biomass in the surface and subsurface layers of the Philippine Sea, where a weak nutrient supply occurred. Our results suggest that *Prochlorococcus* is not controlled by dFe and macronutrient fluxes; a higher abundance of *Prochlorococcus* can be observed in higher water temperatures and lower nutrient supply areas, like the STG. The temperature

is an important factor for controlling this species, as reported in previous studies, rather than dFe and macronutrient fluxes. Additionally, *Prochlorococcus* are generally expected to deal with lower nutrients due to their small cell size, lower nutrient requirements, and lower maximum growth rates (Partensky et al., 1999). The ecophysiological features of *Prochlorococcus* could make them more adapted or acclimated in the N-limited STG (Fig. 6a) with lower nutrient conditions (Fig. 4a-d).

3.7 Transport of dissolved iron and macronutrients from NPIW to the subsurface layer
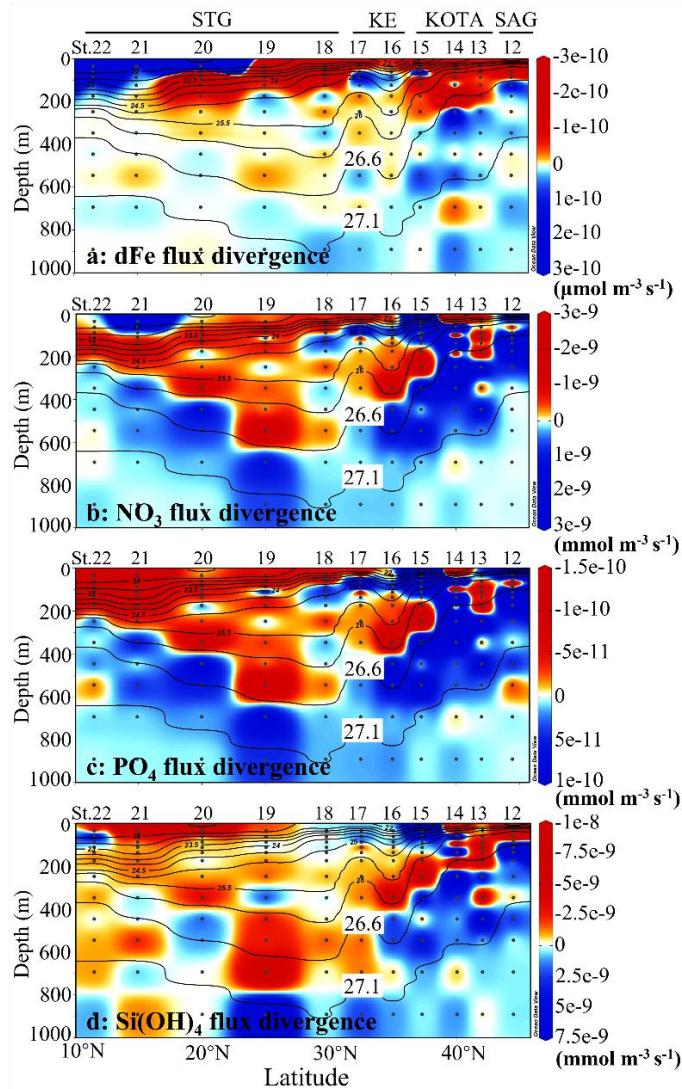
Figure 10: Vertical section profiles of (a) dissolved Fe flux divergence ($\mu mol\ m^{-3}\ s^{-1}$) along 155° E transect from the subarctic to subtropical Pacific, (b) nitrate flux divergence (mmol $m^{-3}\ s^{-1}$), (c) phosphate flux divergence (mmol $m^{-3}\ s^{-1}$) and (d) silicate flux divergence (mmol $m^{-3}\ s^{-1}$). The red and blue colors indicate the convergence and divergence of each nutrient flux, respectively. The highlighted 26.6 and 27.1 σ_θ isopycnal surfaces suggest the shallower and deeper boundaries of the upper NPIW (U-NPIW). These figures were drawn using the ODV.

The dFe flux divergence indicates that water with a density between 26.6 and 27.1 σ_θ has divergence characteristics, and water with a density lower than 26.6 σ_θ has convergence characteristics in the SAG and KOTA. The divergence characteristics indicate a decreasing trend of dFe concentration in the U-NPIW, and the convergence characteristics indicate an increasing trend of dFe concentration in the water above the U-NPIW in the SAG and KOTA. This process suggests a tendency that dFe is supplemented from the U-NPIW to the water above the 26.6 σ_θ isopycnal surface in the SAG and KOTA. Therefore, a relatively low concentration of dFe (Fig. 4a) in the surface layer of the SAG and KOTA implies that dFe would be consumed by phytoplankton in the near-surface water.

The flux divergences of macronutrients (nitrate, phosphate, and silicate) in the SAG and the KOTA show a divergence pattern between 26.6 and 27.1 σ_θ (the U-NPIW). The silicate flux divergence indicates that water above the 26.6 σ_θ isopycnal surface in the SAG and northern part of KOTA at St. 12 and 13 shows a convergence pattern (Fig. 10d). This Si flux convergence tends to increase Si concentration in the surface layer in the similar manner to the dFe pattern in St. 12 and 13. This process indicates that Si is transported from the U-NPIW to the water above 26.6 σ_θ in the SAG and northern part of KOTA at St. 12 and 13. For nitrate and phosphate flux divergence, convergence characteristics can be captured in the water above 26.6 σ_θ in the northern part of KOTA at St. 13 (Fig. 10b, c).

4 Conclusions

In previous studies, phytoplankton abundance was confirmed to be influenced by physical properties, such as light, temperature, and chemical properties, including macronutrient concentration. This study firstly demonstrated strong correlations between dFe or macronutrient fluxes and species-specific Chl *a* concentration, especially for diatoms, in the western North Pacific in summer. The results have revealed that phytoplankton abundance and community composition in the western North Pacific in summer were strongly controlled by dFe and macronutrient fluxes from the subsurface and its stoichiometry. The diatoms were highly regulated by dFe and Si flux from the intermediate water to the surface, as well as the dFe/N flux ratio. Similar to diatoms, haptophytes, and prasinophytes were moderately controlled by dFe and macronutrient fluxes. Fluxes of dFe and macronutrients from the subsurface layers have affected little other phytoplankton communities. Based on the flux divergence estimates, we conclude that the vertical turbulent transport of dFe and silicate from NPIW to the subsurface layer occurs in the subarctic gyre and Kuroshio-Oyashio Transition Area of the western North Pacific, and the dFe and macronutrient supplies significantly control diatom abundance. Our findings contribute to understand oceanic biogeochemical circulation in the North Pacific.

Data availability

The chemical data, including dissolved iron, nitrate, phosphate, and silicate concentration used to produce the figures in this paper, are available from Nishioka et al. (2020) (https://eprints.lib.hokudai.ac.jp/dspace/handle/2115/77482). The physical data, including vertical diffusivity, are publicly available online from Kaneko et al. (2021) (https://ocg.aori.u-tokyo.ac.jp/omix/Kaneko_etal_2020JO/). The biological and CTD data associated with this publication will be deposited in the data archive site of Hokkaido University when the manuscript is accepted.

Author contributions

Each named author has participated sufficiently in the work to take public responsibility for the content. JN, IY, KS developed the concept. JN, KS, IY and HO collected the samples and data. JN, KS and HO analysed the samples. HD and JN analysed the dataset and drafted the manuscript. KS, IY and HO reviewed and edited the manuscript.

Competing interests

Koji Suzuki is a member of the editorial board of Biogeosciences.

Acknowledgements

This cruise, identified as KH-08-2, was supported by the Cooperative Research Program of the Atmosphere and Ocean Research Institute, The University of Tokyo. We thank the crew of the R/V Hakuho-maru for their cooperation and assistance on board.

Financial support

This work was supported by the Ministry of Education, Science, and Culture KAKEN grants B "22H03728 and 23H03516", KAKEN grant A "21H04921" and KAKEN grant S "21H05056". This work was supported by a Grant-in-Aid for Scientific Research "22H05205, 20H05598, 20H04965" and the Grant for Joint Research Program of the Institute of Low Temperature Science, Hokkaido University. The present work was also supported by JST SPRING "JPMJSP2119" and CREST "JPMJCR23J4".

References

Allen, J. T., Brown, L., Sanders, R., Mark Moore, C., Mustard, A., Fielding, S., Lucas, M., Rixen, M., Savidge, G., Henson, S., and Mayor, D.: Diatom carbon export enhanced by silicate upwelling in the northeast Atlantic, Nature, 437, 728–732, https://doi.org/10.1038/nature03948, 2005.

420

Bishop, J. K., Davis, R. E., and Sherman, J. T.: Robotic observations of dust storm enhancement of carbon biomass in the North Pacific, Science, 298, 817-821, https://doi.org/10.1126/science.1074961, 2002.

Boyd, P. W., Law, C. S., Wong, C. S., Nojiri, Y., Tsuda, A., Levasseur, M., Takeda, S., Rivkin, R., Harrison, P. J., Strzepek, 425 R., and Gower, J.: The decline and fate of an iron-induced subarctic phytoplankton bloom, Nature, 428, 549-553, https://doi.org/10.1038/nature02437, 2004.

Boyd, P. W., Mackie, D. S., and Hunter, K. A.: Aerosol iron deposition to the surface ocean—modes of iron supply and biological responses, Mar. Chem., 120, 128-143, https://doi.org/10.1016/j.marchem.2009.01.008, 2010.

430

Boyd, P. W., Watson, A. J., Law, C. S., Abraham, E. R., Trull, T., Murdoch, R., Bakker, D. C., Bowie, A. R., Buesseler, K. O., Chang, H., and Charette, M.: A mesoscale phytoplankton bloom in the polar Southern Ocean stimulated by iron fertilization, Nature, 407, 695-702, https://doi.org/10.1038/35037500, 2000.

435 Coale, K. H., Johnson, K. S., Chavez, F. P., Buesseler, K. O., Barber, R. T., Brzezinski, M. A., Cochlan, W. P., Millero, F. J., Falkowski, P. G., Bauer, J. E., and Wanninkhof, R. H.: Southern Ocean iron enrichment experiment: carbon cycling in high- and low-Si waters, Science, 304, 408-414, https://doi.org/10.1126/science.1089778, 2004.

Coale, K. H., Johnson, K. S., Fitzwater, S. E., Gordon, R. M., Tanner, S., Chavez, F. P., Ferioli, L., Sakamoto, C., Rogers, P., 440 Millero, F., and Steinberg, P.: A massive phytoplankton bloom induced by an ecosystem-scale iron fertilization experiment in the equatorial Pacific Ocean, Nature, 383, 495-501, https://doi.org/10.1038/383495a0, 1996.

Conway, T. M., and John, S. G.: The cycling of iron, zinc and cadmium in the North East Pacific Ocean - Insights from stable isotopes, Geochim. Cosmochim. Ac., 164, 262–283, https://doi.org/10.1016/j.gca.2015.05.023, 2015.

445

Duce, R. A., Liss, P. S., Merrill, J. T., Atlas, E. L., Buat-Menard, P., Hicks, B. B., Miller, J. M., Prospero, J. M., Arimoto, R. C. T. M., Church, T. M., and Ellis, W.: The atmospheric input of trace species to the world ocean, Global Biogeochem. Cy., 5, 193–259, https://doi.org/10.1029/91GB01778, 1991.

450 Endo, H., Hattori, H., Mishima, T., Hashida, G., Sasaki, H., Nishioka, J., and Suzuki, K.: Phytoplankton community responses to iron and CO_2 enrichment in different biogeochemical regions of the Southern Ocean, Polar Biol., 40, 2143-2159, https://doi.org/10.1007/s00300-017-2130-3, 2017.

Endo, H., Ogata, H., and Suzuki, K.: Contrasting biogeography and diversity patterns between diatoms and haptophytes in the
455 central Pacific Ocean, Sci. Rep., 8, 10916, https://doi.org/10.1038/s41598-018-29039-9, 2018.

Endo, H., and Suzuki, K.: Spatial variations in community structure of haptophytes across the Kuroshio front in the Tokara Strait, in Kuroshio Current: Physical, Biogeochemical, and Ecosystem Dynamics, edited by Nagai, T., Saito, H., Suzuki, K., and Takahashi, M., AGU Geophysical Monograph Series, AGU-Wiley, Hoboken, New Jersey, 207–221,
460 https://doi.org/10.1002/9781119428428.ch13, 2019.

FAO: The State of World Fisheries and Aquaculture 2020. Sustainability in action, FAO, Rome, Italy, 244 pp., ISBN 9789251326923, 2020.

465 Favorite, F.: Oceanography of the subarctic Pacific region, 1960–71, in: International North Pacific Fisheries Commission, Bulletin No. 33, Vancouver, B.C., Canada, 1-187, retrieved from http://ci.nii.ac.jp/naid/10015636766, 1976.

Hamm, C. E., Merkel, R., Springer, O., Jurkojc, P., Maier, C., Prechtel, K., and Smetacek, V.: Architecture and material properties of diatom shells provide effective mechanical protection, Nature, 421, 841-843, https://doi.org/10.1038/nature01416,
470 2003.

Hamme, R. C., Webley, P. W., Crawford, W. R., Whitney, F. A., DeGrandpre, M. D., Emerson, S. R., Eriksen, C. C., Giesbrecht, K. E., Gower, J. F., Kavanaugh, M. T., Peña, M. A., Sabine, C. L., Batten, S. D., Coogan, L. A., Grundle, D. S., and Lockwood, D.: Volcanic ash fuels anomalous plankton bloom in subarctic northeast Pacific, Geophys. Res. Lett., 37,
475 https://doi.org/10.1029/2010GL044629, 2010.

Hashioka, T., and Yamanaka, Y.: Seasonal and regional variations of phytoplankton groups by top–down and bottom–up controls obtained by a 3D ecosystem model, Ecol. Model., 202, 68-80, https://doi.org/10.1016/j.ecolmodel.2006.05.038, 2007.

480 Hassler, C. S., and Schoemann, V.: Bioavailability of organically bound Fe to model phytoplankton of the Southern Ocean, Biogeosciences, 6, 2281–2296, https://doi.org/10.5194/bg-6-2281-2009, 2009.

Hirata, T., Hardman-Mountford, N. J., Brewin, R. J. W., Aiken, J., Barlow, R., Suzuki, K., Isada, T., Howell, E., Hashioka, T., Noguchi-Aita, M., and Yamanaka, Y.: Synoptic relationships between surface Chlorophyll-a and diagnostic pigments specific
485 to phytoplankton functional types, Biogeosciences, 8, 311–327, https://doi.org/10.5194/bg-8-311-2011, 2011.

Hogle, S. L., Dupont, C. L., Hopkinson, B. M., King, A. L., Buck, K. N., Roe, K. L., Stuart, R. K., Allen, A. E., Mann, E. L., Johnson, Z. I., and Barbeau, K. A.: Pervasive iron limitation at subsurface chlorophyll maxima of the California Current, P. Natl. Acad. Sci-Biol., 115, 13300-13305, https://doi.org/10.1073/pnas.1813192115, 2018.
490

Holzer, M., DeVries, T., and de Lavergne, C.: Diffusion controls the ventilation of a Pacific Shadow Zone above abyssal overturning, Nat. Commun., 12, 4348, https://doi.org/10.1038/s41467-021-24648-x, 2021.

Huang, B., Liu, C., Banzon, V., Freeman, E., Graham, G., Hankins, B., Smith, T., and Zhang, H. M.: Improvements of the
495 daily optimum interpolation sea surface temperature (DOISST) version 2.1, J. Climate, 34, 2923-2939, https://doi.org/10.1175/JCLI-D-20-0166.1, 2021.

Hutchins, D. A., and Bruland, K. W.: Iron-limited diatom growth and Si: N uptake ratios in a coastal upwelling regime, Nature, 393, 561-564, https://doi.org/10.1038/31203, 1998.
500

Ito, A., Myriokefalitakis, S., Kanakidou, M., Mahowald, N. M., Scanza, R. A., Hamilton, D. S., Baker, A. R., Jickells, T., Sarin, M., Bikkina, S., and Gao, Y.: Pyrogenic iron: The missing link to high iron solubility in aerosols, Sci. Adv., 5, eaau7671, https://doi.org/10.1126/sciadv.aau7671, 2019.

505 Itoh, S., Kaneko, H., Kouketsu, S., Okunishi, T., Tsutsumi, E., Ogawa, H., and Yasuda, I.: Vertical eddy diffusivity in the subsurface pycnocline across the Pacific, J. Oceanogr., 77, 185-197, https://doi.org/10.1007/s10872-020-00589-9, 2021.

Itoh, S., Yasuda, I., Nakatsuka, T., Nishioka, J., and Volkov, Y. N.: Fine- and microstructure observations in the Urup Strait, Kuril Islands, during August 2006, J. Geophys. Res.-Oceans, 115, https://doi.org/10.1029/2009JC005629, 2010.
510

Jickells, T. D., An, Z. S., Andersen, K. K., Baker, A. R., Bergametti, G., Brooks, N., Cao, J. J., Boyd, P. W., Duce, R. A., Hunter, K. A., and Kawahata, H.: Global iron connections between desert dust, ocean biogeochemistry, and climate, Science, 308, 67-71, https://doi.org/10.1126/science.1105959, 2005.

515 Johnson, K. S., Elrod, V., Fitzwater, S., Plant, J., Boyle, E., Bergquist, B., Bruland, K., Aguilar-Islas, A., Buck, K., Lohan, M., Smith, G. J., Sohst, B., Coale, K., Gordon, M., Tanner, S., Measures, C., Moffett, J., Barbeau, K., King, A., Bowie, A., Chase,

Z., Cullen, J., Laan, P., Landing, W., Mendez, J., Milne, A., Obata, H., Doi, T., Ossiander, L., Sarthou, G., Sedwick, P., van den Berg, S., Laglera-Baquer, L., Wu. J., and Cai, Y.: Developing standards for dissolved iron in seawater, Eos Trans. AGU, 88, 131-132, https://doi.org/10.1029/2007EO110003, 2007.

520

Johnson, Z. I., Zinser, E. R., Coe, A., McNulty, N. P., Woodward, E. M. S., and Chisholm, S. W.: Niche partitioning among *Prochlorococcus* ecotypes along ocean-scale environmental gradients, Science, 311, 1737–1740, https://doi.org/10.1126/science.1118052, 2006.

525   Kanayama, T., Kobari, T., Suzuki, K., Yoshie, N., Honma, T., Karu, F., and Kume, G.: Impact of microzooplankton grazing on the phytoplankton community in the Kuroshio of the East China sea: A major trophic pathway of the Kuroshio ecosystem, Deep-Sea Res. Pt. I, 163, 103337, https://doi.org/10.1016/j.dsr.2020.103337, 2020.

Kaneko, H., Yasuda, I., Komatsu, K., and Itoh, S.: Observations of vertical turbulent nitrate flux across the Kuroshio, Geophys.
530   Res. Lett., 40, 3123–3127, https://doi.org/10.1002/grl.50613, 2013.

Kaneko, H., Yasuda, I., Itoh, S., and Ito, S. I.: Vertical turbulent nitrate flux from direct measurements in the western subarctic and subtropical gyres of the North Pacific, J. Oceanogr., 77, 29–44, https://doi.org/10.1007/s10872-020-00576-0, 2021.

535   Kawai, H.: Statistical estimation of isotherms indicative of the Kuroshio axis, Deep-Sea Res., 16, 109–115, 1969.

Kazamia, E., Sutak, R., Paz-Yepes, J., Dorrell, R. G., Vieira, F. R. J., Mach, J., Morrissey, J., Leon, S., Lam, F., Pelletier, E., and Camadro, J. M.: Endocytosis-mediated siderophore uptake as a strategy for Fe acquisition in diatoms, Sci. Adv., 4, p.eaar4536, https://doi.org/10.1126/sciadv.aar4536, 2018.

540

Kurisu, M., Sakata, K., Nishioka, J., Obata, H., Conway, T. M., Hunt, H. R., Sieber, M., Suzuki, K., Kashiwabara, T., Kubo, S., Takada, M., and Takahashi, Y.: Source and fate of atmospheric iron supplied to the subarctic North Pacific traced by stable iron isotope ratios, Geochim. Cosmochim. Ac., 378, 168-185, https://doi.org/10.1016/j.gca.2024.06.009, 2024.

545   Kurisu, M., Sakata, K., Uematsu, M., Ito, A., and Takahashi, Y.: Contribution of combustion Fe in marine aerosols over the northwestern Pacific estimated by Fe stable isotope ratios, Atmos. Chem. Phys., 21, 16027–16050, https://doi.org/10.5194/acp-21-16027-2021, 2021.

Latasa, M.: Improving estimations of phytoplankton class abundances using CHEMTAX, Mar. Ecol. Prog. Ser., 329, 13–21,
550   https://doi.org/10.3354/meps329013, 2007.

Laws, E. A., Pei, S., Bienfang, P., and Grant, S.: Phosphate-limited growth and uptake kinetics of the marine prasinophyte *Tetraselmis suecica* (Kylin) Butcher, Aquaculture, 322, 117-121, https://doi.org/10.1016/j.aquaculture.2011.09.041, 2011.

555 Lewis, M. R., Harrison, W. G., Oakey, N. S., Hebert, D., and Platt, T.: Vertical nitrate fluxes in the oligotrophic ocean, Science, 234(4778), 870–873, https://doi.org/10.1126/science.234.4778.870, 1986.

Li, Z., Sun, D., Wang, S., Huan, Y., Zhang, H., Liu, J., and He, Y.: A global satellite observation of phytoplankton taxonomic groups over the past two decades, Glob. Change Biol., 29, 4511-4529, https://doi.org/10.1111/gcb.16766, 2023.

560

Liefer, J. D., Garg, A., Campbell, D. A., Irwin, A. J., and Finkel, Z. V.: Nitrogen starvation induces distinct photosynthetic responses and recovery dynamics in diatoms and prasinophytes, PLoS One, 13, e0195705, https://doi.org/10.1371/journal.pone.0195705, 2018.

565 Litchman, E., Klausmeier, C. A., Miller, J. R., Schofield, O. M., and Falkowski, P. G.: Multi-nutrient, multi-group model of present and future oceanic phytoplankton communities, Biogeosciences, 3, 585–606, https://doi.org/10.5194/bg-3-585-2006, 2006.

Litchman, E., Klausmeier, C. A., Schofield, O. M., and Falkowski, P. G.: The role of functional traits and trade-offs in 570 structuring phytoplankton communities: scaling from cellular to ecosystem level, Ecol. Lett., 10, 1170-1181, https://doi.org/10.1111/j.1461-0248.2007.01117.x, 2007.

Mackey, M. D., Mackey, D. J., Higgins, H. W., and Wright, S. W.: CHEMTAX - A program for estimating class abundances from chemical markers: Application to HPLC measurements of phytoplankton, Mar. Ecol. Prog. Ser., 144, 265–283, 575 https://doi.org/10.3354/meps144265, 1996.

Martin, J. H., and Fitzwater, S. E.: Iron deficiency limits phytoplankton growth in the north-east Pacific subarctic, Nature, 331, 341-343, https://doi.org/10.1038/331341a0, 1988.

580 Martin, J. H., Fitzwater, S. E., and Gordon, R. M.: Iron deficiency limits phytoplankton growth in Antarctic waters, Global Biogeochem. Cy., 4, 5-12, https://doi.org/10.1029/GB004i001p00005, 1990.

Mills, M. M., Turk-Kubo, K. A., van Dijken, G. L., Henke, B. A., Harding, K., Wilson, S. T., Arrigo, K. R., and Zehr, J. P.: Unusual marine cyanobacteria/haptophyte symbiosis relies on N2 fixation even in N-rich environments, ISME J., 14, 2395-2406, https://doi.org/10.1038/s41396-020-0691-6, 2020.

Misumi, K., Nishioka, J., Obata, H., Tsumune, D., Tsubono, T., Long, M.C., Lindsay, K., and Moore, J. K.: Slowly sinking particles underlie dissolved iron transport across the Pacific Ocean, Global Biogeochem. Cy., 35, e2020GB006823, https://doi.org/10.1029/2020GB006823, 2021.

Nagai, T., Durán, G. S., Otero, D. A., Mori, Y., Yoshie, N., Ohgi, K., Hasegawa, D., Nishina, A., and Kobari, T.: How the Kuroshio Current delivers nutrients to sunlit layers on the continental shelves with aid of near-inertial waves and turbulence, Geophys. Res. Lett., 46, 6726–6735, https://doi.org/10.1029/2019GL082680, 2019.

Nagashima, K., Kawakami, H., Sugie, K., Fujiki, T., Nishioka, J., Iwamoto, Y., Takemura, T., Miyakawa, T., Taketani, F., and Aita, M. N.: Asian dust-deposition flux to the subarctic Pacific estimated using single quartz particles, Sci. Rep., 13, 15424, https://doi.org/10.1038/s41598-023-41201-6, 2023.

Nishioka, J., Takeda, S., Kondo, Y., Obata, H., Doi, T., Tsumune, D., Wong, C. S., Johnson, W. K., Sutherland, N., and Tsuda, A.: Changes in iron concentrations and bio-availability during an open-ocean mesoscale iron enrichment in the western subarctic Pacific, SEEDS II, Deep-sea Res. Pt. II, 56, 2796-2809, https://doi.org/10.1016/j.dsr2.2009.06.006, 2009.

Nishioka, J., Nakatsuka, T., Watanabe, Y. W., Yasuda, I., Kuma, K., Ogawa, H., Ebuchi, N., Scherbinin, A., Volkov, Y. N., Shiraiwa, T., and Wakatsuchi, M.: Intensive mixing along an island chain controls oceanic biogeochemical cycles, Global Biogeochem. Cy., 27, 920–929, https://doi.org/10.1002/gbc.20088, 2013.

Nishioka, J., and Obata, H.: Dissolved iron distribution in the western and central subarctic Pacific: HNLC water formation and biogeochemical processes, Limnol. Oceanogr., 62, 2004–2022, https://doi.org/10.1002/lno.10548, 2017.

Nishioka, J., Obata, H., Hirawake, T., Kondo, Y., Yamashita, Y., Misumi, K., and Yasuda, I.: A review: iron and nutrient supply in the subarctic Pacific and its impact on phytoplankton production, J. Oceanogr., 77, 561-587, https://doi.org/10.1007/s10872-021-00606-5, 2021.

Nishioka, J., Obata, H., Ogawa, H., Ono, K., Yamashita, Y., Lee, K., Takeda, S., and Yasuda, I.: Subpolar marginal seas fuel the North Pacific through the intermediate water at the termination of the global ocean circulation, P. Natl. Acad. Sci. USA, 117, 12665–12673, https://doi.org/10.1073/pnas.2000658117, 2020.

Nishioka, J., Ono, T., Saito, H., Nakatsuka, T., Takeda, S., Yoshimura, T., Suzuki, K., Kuma, K., Nakabayashi, S., Tsumune, D., and Mitsudera, H.: Iron supply to the western subarctic Pacific: Importance of iron export from the Sea of Okhotsk, J. Geophys. Res.-Oceans, 112, https://doi.org/10.1029/2006JC004055, 2007.

Nishioka, J., Ono, T., Saito, H., Sakaoka, K., and Yoshimura, T.: Oceanic iron supply mechanisms which support the spring diatom bloom in the Oyashio region, western subarctic Pacific, J. Geophys. Res.-Oceans, 116, https://doi.org/10.1029/2010JC006321, 2011.

Nodwell, L. M., and Price, N. M.: Direct use of inorganic colloidal iron by marine mixotrophic phytoplankton, Limnol. Oceanogr., 46, 765-777, https://doi.org/10.4319/lo.2001.46.4.0765, 2001.

Obata, H., Karatani, H., and Nakayama, E.: Automated determination of iron in seawater by chelating resin concentration and chemiluminescence detection, Anal. Chem., 65, 1524–1528, https://doi.org/10.1021/ac00059a007, 1993.

Osborn, T. R.: Estimates of the local rate of vertical diffusion from dissipation measurements, J. Phys. Oceanogr., 10, 83–89, https://doi.org/10.1175/1520-0485(1980)010<0083:eotlro>2.0.co;2, 1980.

Partensky, F., Hess, W. R., and Vaulot, D.: *Prochlorococcus*, a marine photosynthetic prokaryote of global significance. Microbiol. Mol. Ecol. Rev., 63, 106-127, https://doi.org/10.1128/mmbr.63.1.106-127.1999, 1999.

Rae, J. W., Gray, W. R., Wills, R. C. J., Eisenman, I., Fitzhugh, B., Fotheringham, M., Littley, E. F. M., Rafter, P. A., Rees-Owen, R., Ridgwell, A., and Taylor, B.: Overturning circulation, nutrient limitation, and warming in the Glacial North Pacific, Sci. Adv., 6, eabd1654, https://doi.org/10.1126/sciadv.abd1654, 2020.

Reid, J. L.: Intermediate waters of the Pacific Ocean, Johns Hopkins Press, Baltimore, Maryland, 85pp, ISBN 0801805465, 1965.

Rii, Y. M., Bidigare, R. R., and Church, M. J.: Differential responses of eukaryotic phytoplankton to nitrogenous nutrients in the North Pacific Subtropical Gyre, Front. Mar. Sci, 5, 92, https://doi.org/10.3389/fmars.2018.00092, 2018.

Sarmiento, J. L., Gruber, N., Brzezinski, M. A., and Dunne, J. P.: High-latitude controls of thermocline nutrients and low latitude biological productivity, Nature, 427, 56–60, https://doi.org/10.1038/nature02127, 2004.

Sarmiento, J. L., and Gruber, N.: Ocean Biogeochemical Dynamics, Princeton University Press, Princeton, New Jersey, https://doi.org/10.2307/j.ctt3fgxqx, 2006.

655 Shimada, C., Tanaka, Y., and Tanimura, Y.: Seasonal variation in skeletal silicification of Neodenticula seminae, a marine planktonic diatom: sediment trap experiments in the NW Pacific Ocean (1997–2001), Mar. Micropaleontol., 60, 130-144, https://doi.org/10.1016/j.marmicro.2006.04.006, 2006.

Sommer, U.: The paradox of the plankton: Fluctuations of phosphorus availability maintain diversity of phytoplankton in flow-through cultures 1, Limnol. Oceanogr., 29, 633-636, https://doi.org/10.4319/lo.1984.29.3.0633, 1984.

660

Sunda, W. G., and Huntsman, S. A.: Iron uptake and growth limitation in oceanic and coastal phytoplankton, Mar. Chem., 50, 189-206, https://doi.org/10.1016/0304-4203(95)00035-P, 1995.

Suzuki, K., Handa, N., Kiyosawa, H., and Ishizaka, J.: Distribution of the prochlorophyte Prochlorococcus in the central Pacific
665 as measured by HPLC, Limnol. Oceanogr., 40, 983-989, https://doi.org/10.4319/lo.1995.40.5.0983, 1995.

Suzuki, K., Kuwata, A., Yoshie, N., Shibata, A., Kawanobe, K., and Saito, H.: Population dynamics of phytoplankton, heterotrophic bacteria, and viruses during the spring bloom in the western subarctic Pacific, Deep-Sea Res. Pt. I, 58, 575-589, https://doi.org/10.1016/j.dsr.2011.03.003, 2011.

670

Suzuki, K., Hattori-Saito, A., Sekiguchi, Y., Nishioka, J., Shigemitsu, M., Isada, T., Liu, H., and McKay, R. M. L.: Spatial variability in iron nutritional status of large diatoms in the Sea of Okhotsk with special reference to the Amur River discharge, Biogeosciences, 11, 2503–2517, https://doi.org/10.5194/bg-11-2503-2014, 2014.

675 Suzuki, K., Saito, H., Isada, T., Hattori-Saito, A., Kiyosawa, H., Nishioka, J., McKay, R. M. L., Kuwata, A., and Tsuda, A.: Community structure and photosynthetic physiology of phytoplankton in the northwest subarctic Pacific during an in situ iron fertilization experiment (SEEDS-II), Deep-Sea Res. Pt. II, 56, 2733-2744, https://doi.org/10.1016/j.dsr2.2009.06.001, 2009.

Suzuki, K., Minami, C., Liu, H., and Saino, T.: Temporal and spatial patterns of chemotaxonomic algal pigments in the
680 subarctic Pacific and the Bering Sea during the early summer of 1999, Deep-Sea Res. Pt. II, 49, 5685–5704, https://doi.org/10.1016/S0967-0645(02)00218-7, 2002.

Suzuki, K., Yoshino, Y., Nosaka, Y., Nishioka, J., Hooker, S. B., and Hirawake, T.: Diatoms contributing to new production in surface waters of the northern Bering and Chukchi Seas during summer with reference to water column stratification, Prog.

685 Oceanogr., 199, 102692, https://doi.org/10.1016/j.pocean.2021.102692, 2021.

Takahashi, Y., Furukawa, T., Kanai, Y., Uematsu, M., Zheng, G., and Marcus, M. A.: Seasonal changes in Fe species and soluble Fe concentration in the atmosphere in the Northwest Pacific region based on the analysis of aerosols collected in Tsukuba, Japan, Atmos. Chem. Phys., 13, 7695-7710, https://doi.org/10.5194/acp-13-7695-2013, 2013.

690

Takeda, S.: Iron and Phytoplankton Growth in the Subarctic North Pacific, Aqua-BioSci. Monogr., 4, 41–93, https://doi.org/10.5047/absm.2011.00402.0041, 2011.

Tanaka, T., Hasegawa, D., Yasuda, I., Tsuji, H., Fujio, S., Goto, Y., and Nishioka, J.: Enhanced vertical turbulent nitrate flux

695 in the Kuroshio across the Izu Ridge, J. Oceanogr., 75, 195–203, https://doi.org/10.1007/s10872-018-0500-2, 2019.

Tsuda, A., Takeda, S., Saito, H., Nishioka, J., Nojiri, Y., Kudo, I., Kiyosawa, H., Shiomoto, A., Imai, K., Ono, T., and Shimamoto, A.: A mesoscale iron enrichment in the western subarctic Pacific induces a large centric diatom bloom, Science, 300, 958–961, https://doi.org/10.1126/science.1082000, 2003.

700

Wang, Y., Bi, R., Zhang, J., Gao, J., Takeda, S., Kondo, Y., Chen, F., Jin, G. E., Sachs, J. P., and Zhao, M.: Phytoplankton distributions in the Kuroshio-Oyashio region of the Northwest Pacific Ocean: Implications for marine rcology and carbon cycle, Front. Mar. Sci., 9, 865142, https://doi.org/10.3389/fmars.2022.865142, 2022.

705 Welschmeyer, N. A.: Fluorometric analysis of chlorophyll a in the presence of chlorophyll b and pheopigments, Limnol. Oceanogr., 39, 1985-1992, https://doi.org/10.4319/lo.1994.39.8.1985, 1994.

Yamashita, Y., Nishioka, J., Obata, H., and Ogawa, H.: Shelf humic substances as carriers for basin-scale iron transport in the North Pacific, Sci. Rep., 10, 4505, https://doi.org/10.1038/s41598-020-61375-7, 2020.

710

Yasuda, I., Hiroe, Y., Komatsu, K., Kawasaki, K., Joyce, T. M., Bahr, F., and Kawasaki, Y.: Hydrographic structure and transport of the Oyashio south of Hokkaido and the formation of North Pacific Intermediate Water, J. Geophys. Res.-Oceans, 106, 6931–6942, https://doi.org/10.1029/1999jc000154, 2001.

715 Yoshida, M., Noël, M. H., Nakayama, T., Naganuma, T., and Inouye, I.: A haptophyte bearing siliceous scales: ultrastructure and phylogenetic position of Hyalolithus neolepis gen. et sp. nov. (Prymnesiophyceae, Haptophyta), Protist, 157, 213-234, https://doi.org/10.1016/j.protis.2006.02.004, 2006.

Yun, M. S., Kim, Y., Jeong, Y., Joo, H. T., Jo, Y. H., Lee, C. H., Bae, H., Lee, D., Bhavya, P. S., Kim, D., and Sun, J.: Weak
720 response of biological productivity and community structure of phytoplankton to mesoscale eddies in the oligotrophic Philippine Sea, J. Geophys. Res.-Oceans, 125, e2020JC016436, https://doi.org/10.1029/2020JC016436, 2020.

Zubkov, M. V., Sleigh, M. A., Burkill, P. H., and Leakey, R. J.: Picoplankton community structure on the Atlantic Meridional Transect: a comparison between seasons, Prog. Oceanogr., 45, 369-386, https://doi.org/10.1016/S0079-6611(00)00008-2,
725 2000.